ELSEVIER

Nuclear Physics B 493 (1997) 56–72

NUCLEAR PHYSICS B

Single-photon Z decays and small neutrino masses

J.C. Romão [a,1], S.D. Rindani [b,2], J.W.F. Valle [b]

[a] *Inst. Superior Técnico, Dept. de Física, Av. Rovisco Pais, 1, 1096 Lisboa, Codex, Portugal*

[b] *Instituto de Física Corpuscular - C.S.I.C., Departament de Física Teòrica, Universitat de València, 46100 Burjassot, València, Spain* [3]

Received 9 December 1996; accepted 20 February 1997

Abstract

We discuss some rare Z decay signatures associated with extensions of the Standard Model with spontaneous lepton number violation close to the weak scale. We show that single-photon Z decays such as $Z \to \gamma H$ and $Z \to \gamma JJ$ where H is a CP-even Higgs boson and J denotes the associated CP-odd majoron may occur with branching ratios accessible to LEP sensitivities, even though the corresponding neutrino masses can be very small, as required in order to explain the deficit of solar neutrinos. © 1997 Elsevier Science B.V.

1. Introduction

There is a large variety of ways to generate naturally small neutrino masses which do not require one to introduce a large mass scale [1]. In some of these models the neutrinos acquire mass only through radiative corrections [2,3]. In addition to their potential in explaining present puzzles in neutrino physics [4], such as that of solar and atmospheric neutrinos [5], such models may give rise to many new signals at high-energy accelerator experiments [6].

Here we consider *radiative* schemes of neutrino mass generation. For definiteness we focus on that introduced in Ref. [3] where neutrino masses are induced at the two-loop level. For our purposes this model will be the simplest, as it does not contain any scalar Higgs doublet in addition to that of the standard model. Following Ref. [7], we slightly

[1] E-mail: fromao@alfa.ist.utl.pt

[2] Permanent address: Theory Group, Physical Research Laboratory, Navarangpura, Ahmedabad, 380 009, India.

[3] http://neutrinos.uv.es

PII S0550-3213(97)00167-3

generalize the model adding a new singlet scalar boson σ carrying two units of lepton number, so that this symmetry is broken spontaneously. This leads to the existence of a physical Goldstone boson, called majoron, denoted J. One feature worth noting here is that, although the majoron has very tiny couplings to matter and gauge bosons (in particular, it gives no contribution to the invisible Z decay width), it can have significant couplings to the Higgs bosons. Since the scale at which the lepton number symmetry gets broken in this model lies close to the weak scale, there is a variety of possible phenomenological implications, such as a substantial Higgs boson decay branching ratio into the invisible channel [8]

$$H \to J + J. \tag{1}$$

In this paper we consider the signatures associated with the single-photon Z boson decays such as

$$Z \to \gamma H, \qquad Z \to \gamma J, \qquad Z \to \gamma JJ, \tag{2}$$

where H is a CP-even Higgs boson, and J denotes the associated CP-odd majoron. We have calculated the possible values allowed for these decay branching ratios within a specific model for neutrino mass proposed in Ref. [7] and which generalizes the one first proposed in Ref. [3] by introducing the majoron. Since the majoron J is weakly coupled to the rest of the particles, once produced in the accelerator, it will escape detection, leading to a missing energy signal for the Higgs boson [8,9]. In the present context the invisible majoron will give rise to the single-photon Z-decay signal

$$Z \to \gamma \not{E}_T. \tag{3}$$

It is interesting to notice that single-photon events have been recorded at LEP which apparently can not be ascribed to standard model processes [10].

We have shown that the branching ratios for the decays $Z \to \gamma H$ and the Higgs-mediated decay $Z \to \gamma JJ$ can reach values comparable with LEP sensitivities at the Z pole. It is remarkable that such sizeable values occur even though the associated neutrino masses are very small, as required in order to explain the deficit of solar neutrinos through the resonant conversion effect [11]. This happens due to the fact that neutrino masses are induced only radiatively, at the two-loop level. This is in sharp contrast to the conventional majoron model formulated in the seesaw context, where a large scale is introduced in order to account for the smallness of neutrino masses [12].

2. The model

We consider a modification of the model for radiative neutrino masses first proposed in [3] to incorporate spontaneous breaking of global lepton number, leading to a majoron.

The model is based on the gauge group $SU(2) \times U(1)$, with the same fermion content as that of the standard model, but three complex singlets of scalars in addition to the

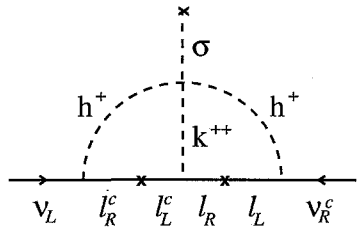

Fig. 1. Two-loop-induced neutrino mass.

doublet. Thus the quark sector is standard and no right-handed neutrino is introduced. Of the three complex singlets, two are charged, viz., $h^{\pm}$ with charge ± 1 and lepton number ∓ 2, and $k^{\pm\pm}$ with charge ± 2 and lepton number ∓ 2. The third neutral singlet scalar σ carries lepton number 2 and is introduced so as to conserve lepton number in the full Lagrangian, including the scalar self-interactions [7].

With the choice of scalars and the representations which we have made, the most general Yukawa interactions of the leptons can be written as

$$\mathcal{L} = -\frac{\sqrt{2}m_i}{v}\bar{\ell}_i \phi e_{Ri} + f_{ij}\ell_i^T C i\tau_2 \ell_j h^+ + h_{ij} e_{Ri}^T C e_{Rj} k^{++} + \text{H.c.}, \tag{4}$$

where h and f are symmetric and anti-symmetric coupling matrices, respectively. The lepton masses are generated when the $SU(2) \otimes U(1)$ gauge symmetry is broken by $\langle\phi\rangle$. The first term gives the charged lepton masses m_i at the tree level, while neutrinos acquire masses radiatively, at the two-loop level, by the diagram in Fig. 1. For reasonable and natural choices of parameters, consistent with all present observations, e.g. $f_{e\tau}, f_{\mu\tau}, h_{\tau\tau} \sim 0.01$, the singlet vacuum expectation value of about 100 GeV, and charged Higgs boson masses of about 100 GeV, these neutrino masses are in the 10^{-2} to 10^{-3} eV range, where they could explain the deficit of solar neutrinos through the resonant conversion effect [11].

3. The scalar potential

The most general scalar potential which is invariant under the gauge group and under global lepton number, with at most quartic terms, is

$$\begin{aligned} V(\phi, h, k, \sigma) = {} & \mu_1^2 \phi^\dagger \phi + \mu_2^2 h^+ h^- + \mu_3^2 k^{++} k^{--} + \mu_0^2 \sigma^* \sigma \\ & + \lambda_1 (\phi^\dagger \phi)^2 + \lambda_2^2 (h^+ h^-)^2 + \lambda_3 (k^{++} k^{--})^2 + \lambda_0 (\sigma^* \sigma)^2 \\ & + \lambda_4 (\phi^\dagger \phi)(h^+ h^-) + \lambda_5 (\phi^\dagger \phi)(k^{++} k^{--}) + \lambda_6 (h^+ h^-)(k^{++} k^{--}) \\ & + \lambda_7 (\phi^\dagger \phi)(\sigma^* \sigma) + \lambda_8 (h^+ h^-)(\sigma^* \sigma) + \lambda_9 (k^{++} k^{--})(\sigma^* \sigma) \\ & + \lambda_0 h^+ h^+ k^{--} \sigma + \lambda_0^* h^- h^- k^{++} \sigma^*. \end{aligned} \tag{5}$$

We assume that for a choice of parameters of the potential, both the $SU(2) \otimes U(1)$ gauge symmetry as well as the global lepton number symmetry are broken spontaneously,

with the neutral scalar fields getting vacuum expectations values. We rewrite the neutral fields as follows:

$$\phi^0 = \frac{1}{\sqrt{2}}(v + \phi_R^0 + i\phi_I^0), \tag{6}$$

$$\sigma = \frac{1}{\sqrt{2}}(\omega + \sigma_R + i\sigma_I). \tag{7}$$

v and ω are the vacuum expectation values defined by[4]

$$\langle\phi^0\rangle = \frac{v}{\sqrt{2}}, \tag{8}$$

$$\langle\sigma\rangle = \frac{\omega}{\sqrt{2}}. \tag{9}$$

The physical massive scalars which survive are those corresponding to $h^{\pm}$, $k^{\pm\pm}$, and two orthogonal combinations of ϕ_R^0 and σ_R. The charged components of ϕ, viz., $\phi^{\pm}$, correspond to the would-be Goldstone particles absorbed by $W^{\pm}$, ϕ_I^0 is the would-be Goldstone eaten by the Z boson and σ_I is the massless physical Goldstone field corresponding to spontaneously broken global lepton number.

We can write the following expressions for the squared masses of the various scalars:

$$M_{h^+}^2 = \mu_2^2 + \tfrac{1}{2}\lambda_4 v^2 + \tfrac{1}{2}\lambda_8\omega^2, \tag{10}$$

$$M_{k^{++}}^2 = \mu_3^2 + \tfrac{1}{2}\lambda_5 v^2 + \tfrac{1}{2}\lambda_9\omega^2. \tag{11}$$

The squared mass terms for the neutral scalars can be written as $-\frac{1}{2}\Phi_i M_{ij}^2 \Phi_j + \ldots$ where we have defined the vector

$$\Phi = \begin{bmatrix} \phi_R^0 \\ \sigma_R \end{bmatrix}. \tag{12}$$

The squared mass matrix M^2 is given by

$$M^2 = \begin{bmatrix} 2\lambda_1\, v^2 & \lambda_7\, \omega v \\ \lambda_7\, \omega v & 2\lambda_0\, \omega^2 \end{bmatrix}. \tag{13}$$

The mass eigenstates are H_i defined through

$$H_i = P_{ij}\Phi_j, \tag{14}$$

where the diagonalization matrix P is orthogonal, that is, $P^{-1} = P^T$. Therefore the inverse of Eq. (14) reads

$$\Phi_i = P_{ji}\, H_j, \tag{15}$$

or in terms of the fields ϕ_R^0 and σ_R,

$$\begin{cases} \phi_R^0 = P_{11}\, H_1 + P_{21}\, H_2, \\ \sigma_R = P_{12}\, H_1 + P_{22}\, H_2. \end{cases} \tag{16}$$

[4] Our choice of the ϕ vacuum expectation value differs from that in [3] by a factor of $\sqrt{2}$.

Before we close this section let us derive two important relations. In the basis Φ_i the eigenvectors H_i have components

$$\begin{bmatrix} P_{i1} \\ P_{i2} \end{bmatrix}. \tag{17}$$

Therefore the eigenvalue equation reads

$$M^2 H_i = M^2_{H_i} H_i, \quad i = 1,2 \tag{18}$$

which gives explicitly

$$\begin{aligned} &2\lambda_1 v^2 P_{i1} + \lambda_7 \omega v P_{i2} = M^2_{H_i} P_{i1}, \\ &\lambda_7 \omega v P_{i1} + 2\lambda_0 \omega^2 P_{i2} = M^2_{H_i} P_{i2}. \end{aligned} \tag{19}$$

These expressions will be useful below.

4. The calculation of the single-photon processes

In this section we will describe the relevant couplings which are different from the ones in standard model, or are new. The couplings of the physical and unphysical scalars among themselves are simply obtained by substituting from Eqs. (6) and (7) into the scalar potential given by Eq. (5), and making use of Eqs. (19) and (16). The relevant terms in the Lagrangian resulting from this substitution are

$$\begin{aligned} -\mathcal{L} =& \phi^+ \phi^- H_i \frac{M^2_{H_i}}{v} P_{i1} + \tfrac{1}{2} J^2 H_i \frac{M^2_{H_i}}{\omega} P_{i2} \\ &+ \tfrac{1}{2} J^2 \left[\lambda_7 \phi^+ \phi^- + \lambda_8 h^+ h^- + \lambda_9 k^{++} k^{--} \right] + \ldots \end{aligned} \tag{20}$$

The unphysical scalars $\phi^\pm$ have exactly the same couplings to the gauge fields and the Faddeev–Popov ghosts as in the standard model, whereas the couplings of the neutral massive scalars, H_i, are obtained by multiplying the standard model couplings, written in terms of the physical masses, by P_{i1}. For example, the coupling of H_i to W^+W^- is given by

$$\mathcal{L} = g M_W P_{i1} W^+_\mu W^{-\mu} H_i. \tag{21}$$

The charged physical scalars h and k have the following couplings to the gauge bosons:

$$\begin{aligned} \mathcal{L} =& -ie(A_\mu + \tan\theta_W Z_\mu) \left\{ (h^- \partial_\mu h^+ - \partial_\mu h^- h^+) \right. \\ &\left. + 2(k^{--} \partial_\mu k^{++} - \partial_\mu k^{--} k^{++}) \right\} \\ &+ e^2 (A_\mu + \tan\theta_W Z_\mu)^2 (h^+ h^- + 4 k^{++} k^{--}). \end{aligned} \tag{22}$$

In order to estimate the branching ratios for the single-photon processes in our model we have varied the values of M_{H_2}, of $M_{h^\pm}$, of $M_{k^{\pm\pm}}$ in the 100 GeV range, and the quartic couplings in the potential over the range

$$0 \leqslant \lambda_{\text{quartic}} \leqslant \sqrt{4\pi}, \tag{23}$$

while the lepton number violation scale ω and CP-even Higgs mixing angle θ were chosen in the range

$$\begin{aligned} 2 &\leqslant \frac{v}{\omega} \leqslant 3, \\ 0 &\leqslant \theta \leqslant \frac{\pi}{2}. \end{aligned} \tag{24}$$

We have also studied the effect having lower values for the lepton number violation scale ω, and obtained a slight enhancement of our branching ratios for the single-photon processes. Notice that with our conventions we have for the mixing matrix of the CP-even Higgs bosons

$$P = \begin{bmatrix} \cos\theta & -\sin\theta \\ \sin\theta & \cos\theta \end{bmatrix}. \tag{25}$$

4.1. The $Z \to H\gamma$ decay

This process arises from the Feynman diagrams shown in Fig. 2. In addition to standard model diagrams this process receives contributions from the new physical singly as well doubly charged scalar bosons, as shown in Fig. 2. The amplitude for the process can be written as

$$\mathcal{M} = \epsilon_Z^{\mu} \epsilon_A^{\nu} \frac{eg^2}{16\pi^2 M_W} \left(g_{\mu\nu} q_1 \cdot q_2 - q_{1\mu} q_{2\nu} \right) A_{H\gamma}, \tag{26}$$

where q_1 and q_2 are the photon and Higgs momenta, respectively. The normalized amplitude $A_{H\gamma}$ is given by

$$A_{H\gamma} = A_{\text{SM}} P_{11} + A_h + A_k, \tag{27}$$

where A_{SM} is the corresponding amplitude for the standard model and A_h and A_k are the amplitudes corresponding to the loops of the new charged scalars. We give their explicit expressions in Appendix A.

The resulting $Z \to \gamma H$ decay width is then

$$\Gamma = \frac{1}{12\pi} \left(\frac{eg^2}{16\pi^2 M_W} \right)^2 E_\gamma^3 |A_{H\gamma}|^2, \tag{28}$$

where $E_\gamma = (M_Z^2 - M_h^2)/(2M_Z)$ is the energy of the photon.

As an illustrative example we show in Fig. 3 the expected branching ratio branching ratio for $Z \to \gamma H$ as a function of M_H for the standard model and for our model.[5] In this figure we have taken $M_{H_2} = 100$ GeV and $M_{h^\pm} = M_{k^{\pm\pm}} = 70$ GeV. For reasonable allowed choices of the relevant parameters one sees that the value of this branching

[5] In the present model we also denote M_H the mass of the lightest CP-even Higgs boson H_1.

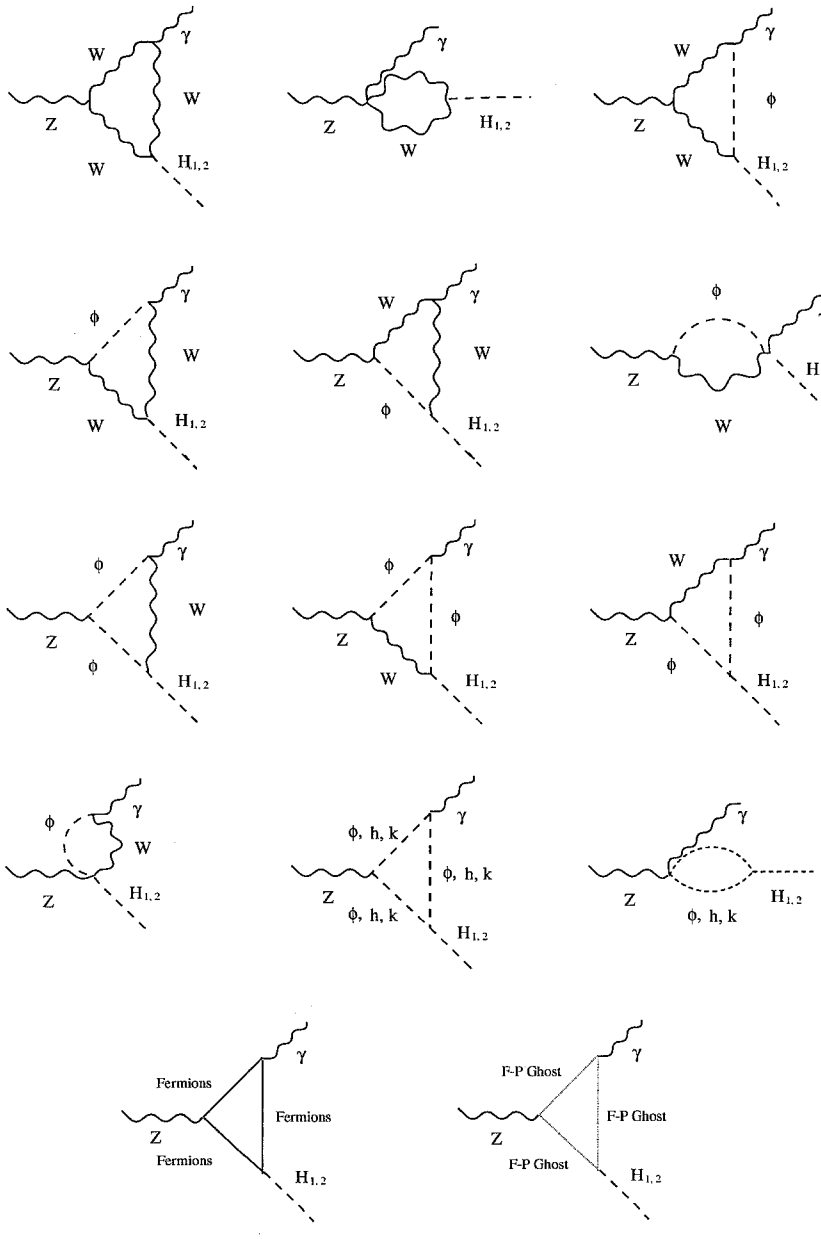

Fig. 2. Feynman diagrams for the decay $Z \to H\gamma$.

ratio can be enhanced with respect to the standard model predictions, but only slightly, by a factor 2 or so, for any fixed M_H. The most novel aspect of this decay in the present model comes from the fact that the CP-even Higgs boson H may decay into two majorons with a substantial branching ratio, leading to a mono-photon plus missing energy signature for the decay $Z \to H\gamma$.

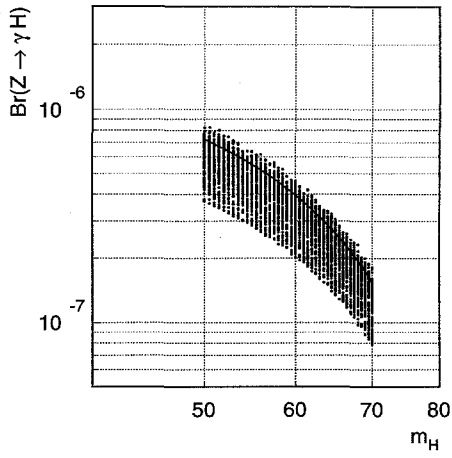

Fig. 3. Branching ratio for $Z \to \gamma H$ as a function of M_H for the standard model (solid line) and for our model (points).

4.2. *Majoron emitting Z decays*

The majoron does not couple to the Z boson at the tree level, since it is an $SU(2) \otimes U(1)$ singlet. Nevertheless it can couple radiatively leading, for example, to processes such as $Z \to \gamma J$ and $Z \to \gamma + J + J$, recently discussed in a different context in Ref. [13]. These processes are, of course, absent in the standard model.

The single-majoron emission process would give rise to a characteristic signature consisting of monochromatic photons plus missing energy. In contrast to the model considered in Ref. [13], the single-majoron emission process is expected to be very small in the present model. Notice, for example, that since the majoron does not couple to charged leptons at the tree level, the one-loop diagram involving charged lepton exchange is absent.

In contrast the process $Z \to \gamma JJ$ proceeds at the one-loop level through two types of diagrams. The first set of diagrams involves the one-loop coupling of Z to γ and H_i (which may be off-shell), with a tree-level coupling of H_i to two majorons, Fig. 4. In the other set of diagrams, Fig. 5, the two majorons arise from a quartic coupling to a pair of charged scalars ($\phi^{\pm}$, $h^{\pm}$ or $k^{\pm\pm}$). The first set is directly related to the set of diagrams for the process $Z \to \gamma H_1$ discussed in Section 4.1, and can be computed simply by first replacing the Higgs boson H_1 by H_i, then multiplying the corresponding amplitude by the propagator for the field H_i, and finally summing over $i = 1, 2$. The particles running in the loops are, in this case, not only those present in the standard model but also the charged scalars $h^{\pm}$ and $k^{\pm\pm}$. The corresponding amplitudes have been calculated in Section 4.1. The second set of diagrams correspond to the quartic couplings of the majorons to the charged scalars. It can be shown that the first diagram of Fig. 5 is not gauge invariant but exactly cancels against the non-gauge invariant part of the diagrams in Fig. 4. The remaining diagrams of Fig. 5 with $\phi^{\pm}$, $h^{\pm}$ and $k^{\pm\pm}$

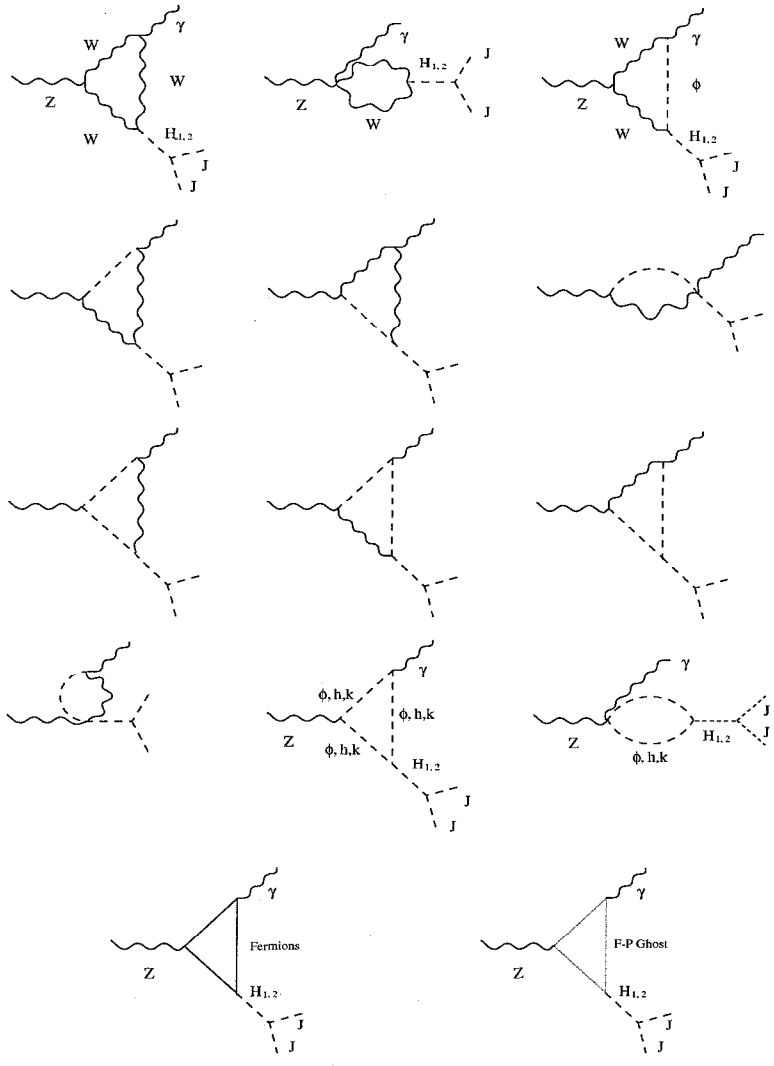

Fig. 4. Feynman diagrams for the H-mediated decay $Z \to \gamma + J + J$.

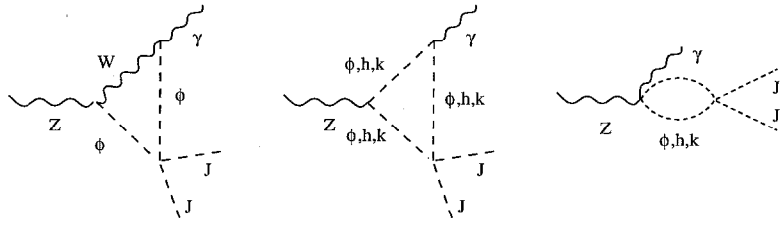

Fig. 5. Additional Feynman diagrams for the decay $Z \to \gamma + J + J$.

running in the loop are gauge invariant by themselves and have to be calculated afresh.

Gauge invariance and CP conservation allow us to write the amplitude for

$$Z(P) \to \gamma(q_1) + J(q_2) + J(q_3) \tag{29}$$

for the case of on-shell Z and γ, as

$$M = \epsilon_\mu^Z \epsilon_\nu^\gamma \frac{eg^2}{16\pi^2 M_W} (g^{\mu\nu} q_1 \cdot Q - q_1^\mu Q^\nu) A_{\gamma JJ}, \tag{30}$$

where $Q = q_2 + q_3$ and use has been made of current conservation for on-shell Z and γ.

The combined contribution of the first set of diagrams to $A_{\gamma JJ}$ can be deduced from the result of Section 4.1. The answer is

$$A_{\gamma JJ}^{(1)} = \sum_{i=1}^{2} \frac{A_{H\gamma}(Q^2)}{Q^2 - M_{H_i}^2 + iM_{H_i}\Gamma_{H_i}} \frac{M_{H_i}^2}{\omega} P_{i2}, \tag{31}$$

where $A_{H\gamma}(Q^2)$ is the amplitude calculated in Section 4.1 evaluated at $Q^2 = (P - q_1)^2 = M_Z(M_Z - 2E_\gamma)$. In Eq. (31) we have introduced the width of H_i, because, as we shall see, the dominant contribution for the process comes when $Q^2 \simeq M_{H_i}^2$.

The contribution to $A_{\gamma JJ}$ of the second set of diagrams can be written as

$$A_{\gamma JJ}^{(2)} = \hat{A}_\phi + \hat{A}_h + \hat{A}_k, \tag{32}$$

where $\hat{A}_\phi$, $\hat{A}_h$ and $\hat{A}_k$ are the contributions of the charged scalars (unphysical and physical) and are given explicitly in Appendix A.

The photon energy spectrum is then

$$\frac{d\Gamma}{dE_\gamma} = \frac{1}{192\pi^3} \left(\frac{e\, g^2}{16\, \pi^2\, M_W} \right)^2 M_Z\, E_\gamma^3 \left| A_{\gamma JJ}^{(1)} + A_{\gamma JJ}^{(2)} \right|^2 \tag{33}$$

and the total width

$$\Gamma = \int_0^{M_Z/2} \frac{d\Gamma}{dE_\gamma} dE_\gamma. \tag{34}$$

We have explicitly verified that the contribution of $A_{\gamma JJ}^{(2)}$ is small when compared with the standard model result for $Z \to H\gamma$. Thus the main contribution comes from the first set of diagrams when $Q^2 \simeq M_{H_i}$. For this reason we need to evaluate the width of H_i. As an approximation, we assume that the doublet part of H_i decays mainly in $\bar{b}b$. In this case we have only two partial widths

$$\Gamma(H_i \to JJ) = \frac{1}{32\pi} \frac{g_{H_iJJ}^2}{M_{H_i}}, \tag{35}$$

$$\Gamma(H_i \to \bar{b}b) = \frac{1}{4\pi} M_{H_i} g_{H_i\bar{b}b}^2 \left(1 - \frac{4m_b^2}{M_{H_i}^2} \right)^{3/2}, \tag{36}$$

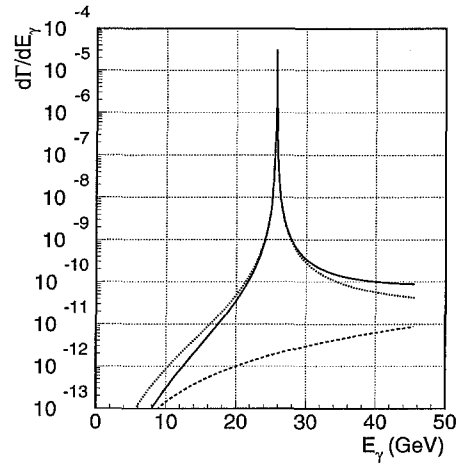

Fig. 6. Photon spectrum for $M_H = 60$ GeV. It is peaked around $E_\gamma \simeq 25.7$ GeV. The solid line represents the total contribution, the dotted line the contribution from the resonant diagrams, and the dashed line the contribution from the non-resonant ones. In this figure we have $M_{H_2} = 100$ GeV and $M_{h^\pm} = M_{k^{\pm\pm}} = 70$ GeV.

where

$$g_{H_iJJ} = \frac{M_{H_i}^2}{\omega} P_{i2}, \qquad g_{H_i\bar{b}b} = \frac{m_b P_{i1}}{v}. \tag{37}$$

As we said before, the photon energy spectrum is peaked around $E_\gamma = (M_Z^2 - M_{H_i}^2)/(2M_Z)$. However, this does not mean that the contribution of the charged scalars is negligible. In fact, we have two extreme cases.

- P_{11} large (small θ).

The dominant contribution comes from the resonant diagrams (first set). The contribution from the loops of charged scalars with quartic vertices is negligible. The energy spectrum is peaked around $E_\gamma = (M_Z^2 - M_H^2)/(2M_Z)$. This can be seen from Fig. 6 which is for $P_{11} = 0.94$. Note that the other diagrams with charged scalars are not negligible because they are also resonant. In fact it is necessary to have them of the same order as the standard model for $Z \to \gamma H$ in order to have an increase. Note also from Fig. 6 that the width of the H_1 is very small. This depends on P_{11} being large as can be seen from Eq. (37) and in Fig. 7.

- P_{11} small (θ close to $\pi/2$).

Now the standard model-like diagrams are small and the main contribution is from the loops of charged scalars. However, the main contribution is still from the resonant charged scalars diagrams. The non-resonant diagrams are small, although not completely negligible. In Fig. 8 we illustrate this for $P_{11} = 0.04$. There we can also see that the width of the H_1 is a few GeV's in agreement with Fig. 7. Note that when $\theta \sim \pi/2$ the branching ratio of the Higgs to JJ is close to one. Thus the standard way of looking for the Higgs, through the standard b–$\bar{b}$ decay mode, would miss it. In the present context this implies that, in addition to the broad photon spectrum in the photon + missing energy signal, one has the additional feature that the $\gamma + b\bar{b}$ signal would be weak.

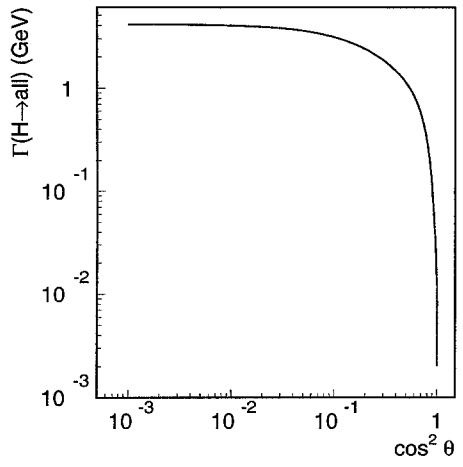

Fig. 7. Upper limits for $\Gamma(H \to all)$ as a function of $P_{11} = \cos^2(\theta)$. In this figure we have $M_{H_2} = 100$ GeV and $M_{h^\pm} = M_{k^{\pm\pm}} = 70$ GeV.

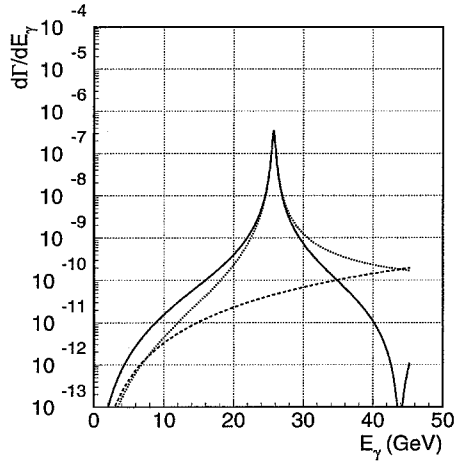

Fig. 8. Photon spectrum for $M_H = 60$ GeV. It is peaked around $E_\gamma \simeq 25.7$ GeV. The solid line represents the total contribution, the dotted line the contribution from the resonant diagrams, and the dashed line the contribution from the non-resonant ones. In this figure we have $M_{H_2} = 100$ GeV and $M_{h^\pm} = M_{k^{\pm\pm}} = 70$ GeV.

The resulting $Z \to \gamma JJ$ decay branching ratio is shown in Fig. 9. Comparing with the results of Fig. 3 we see that the strength of this process is essentially the same as that of $Z \to \gamma H$. This can be easily understood. If we change variables to

$$x = \frac{2 M_Z}{M_H \Gamma_H} E_\gamma, \tag{38}$$

one can, after some simple algebra, write the total width in the form

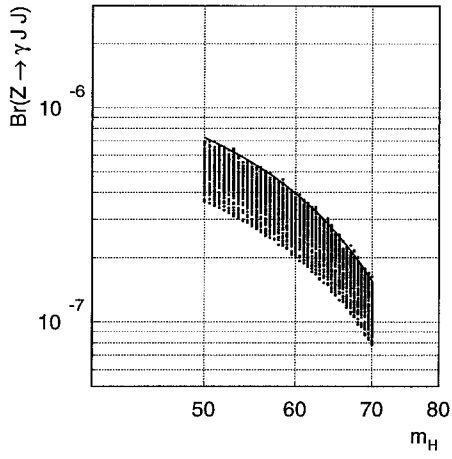

Fig. 9. Width for $Z \to \gamma JJ$ as a function of M_h for our model (points). The standard model result for $Z \to H\gamma$ (solid line) is shown for comparison.

$$\Gamma(Z \to \gamma JJ) = \int_0^{x_{\max}} \Gamma(Z \to H\gamma)\mathrm{Br}(H \to JJ)\frac{1}{\pi}\frac{1}{(x-x_0)^2+1}, \tag{39}$$

where

$$x_{\max} = \frac{M_Z^2}{M_H\Gamma_H}, \tag{40}$$

$$x_0 = \frac{2M_Z}{M_H\Gamma_H}\frac{M_Z^2 - M_H^2}{2M_Z} \tag{41}$$

is the value for which $Q^2 = m_H^2$ in terms of the x variable. Now we notice that

$$\int_{-\infty}^{+\infty} \frac{1}{\pi}\frac{1}{(x-x_0)^2+1} = 1 \tag{42}$$

and if the width is very small we can safely set

$$\frac{1}{\pi}\frac{1}{(x-x_0)^2+1} \simeq \delta(x-x_0) \tag{43}$$

and therefore

$$\Gamma(Z \to \gamma JJ) \simeq \Gamma(Z \to H\gamma)\mathrm{Br}(H \to JJ). \tag{44}$$

One can see from Fig. 10 that the $\mathrm{Br}(H \to JJ)$ is very close to 1 except for the mixing angle in the vicinity of zero as can be understood from Eq. (37).

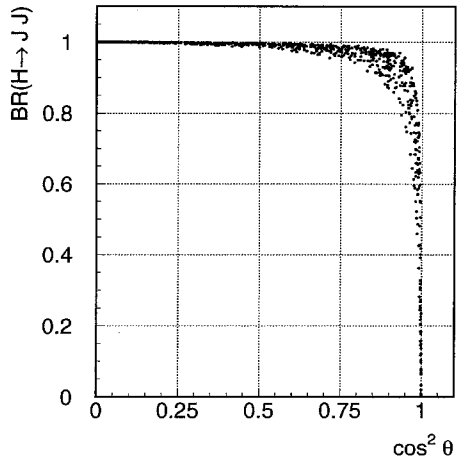

Fig. 10. Br($H \rightarrow JJ$) as a function of $\cos^2\theta$.

5. Discussion

The search for single-photon plus missing energy events constitutes one of the classic experiments in e^+e^- annihilation. Of course, such events are expected to occur through initial state bremsstrahlung with the Z decaying to a $\nu\bar{\nu}$ pair. Recently the OPAL collaboration has published a high-statistics single-photon spectrum that shows some excess of high energy photons above the expectations from initial state radiation [10]. This signal could be an interesting hint for physics beyond the standard model.

In this paper we have studied the rates for single-photon processes such as $Z \rightarrow \gamma H$, $Z \rightarrow \gamma J$ and $Z \rightarrow \gamma JJ$ where H is a massive CP-even Higgs boson, and J denotes the massless (or nearly so) CP-odd majoron associated to the spontaneous violation of lepton number around the weak scale. For this purpose we considered the simple model proposed in Ref. [7]. We have demonstrated that in this simple model the $Z \rightarrow \gamma H$ and $Z \rightarrow \gamma JJ$ decays may occur with branching ratios compatible with LEP sensitivities. That such indirect signals of models of neutrino mass can be sizeable is quite remarkable, taking into account that the corresponding neutrino masses themselves are very small, as required in order to explain the solar neutrino problem. In the model in question the smallness of the neutrino masses follows naturally from the fact that they arise only at the two-loop level.

The γ spectrum associated to these decays is shown in Figs. 6 and 8. It is characterized by a spike located at a photon energy $E_\gamma = (M_Z^2 - M_H^2)/(2M_Z)$, determined by the possible values of the scalar Higgs boson masses M_H. The constraints on M_H that follow from the LEP100 experiments differ from those obtained in the standard model since (i) the CP-even Higgs boson neutral-current couplings are somewhat suppressed due to the admixture of the singlet required to implement the spontaneous violation of lepton number and (ii) these CP-even Higgs bosons can decay with substantial rates into the invisible channel JJ [9]. Here we showed explicitly how the invisible Higgs

decay can be important also in conjunction with radiative $Z \to \gamma H$ decays, leading to a sizeable rate for the $Z \to \gamma \not{E}_T$ signal on the Z peak.

While LEP200 will play an important role in searching for invisibly decaying Higgs bosons [14], high statistics studies of the single-photon energy spectrum at the Z pole may still be an interesting physics goal, as illustrated through the model described in this paper.

We now comment on whether one could distinguish between different models for enhanced single-photon events, using the photon spectrum. Unfortunately, this seems difficult. First, let us consider to what extent the branching ratios and spectra calculated depend on the model, for example supersymmetric models with spontaneous R-parity violation [13]. In this case the main contribution for $Z \to \gamma JJ$ will come again from the resonant diagrams, because the box diagrams are very small. Also the diagrams corresponding to our Fig. 5 (only with the Higgs doublet ϕ) are small, in fact they are included in the usual standard model calculation. Thus it is clear that one gets the same type of results, as long as the lightest Higgs boson invisible decay branching ratio $\mathrm{Br}(H \to JJ)$ is close to 100%. One difference will be that, since in this case we do not have the contribution from $h^{\pm}$ and $k^{\pm\pm}$, the result will be always *smaller* than in the Standard Model, though probably close. Note that, since in the supersymmetric case the main process $Z \to H\gamma$ gets contributions from charginos, it could be bigger than in the Standard Model, though of the same order of magnitude. In this case $Z \to \gamma JJ$ could also be bigger. As far as the spectra are concerned, they will be very similar, since the diagrams that could change them, like the boxes or those of Fig 5 will be small. These issues will be taken up elsewhere.

Acknowledgements

This work has been supported by DGICYT under Grants PB95-1077 and SAB95-0175 (S.D.R.), by the TMR network grant ERBFMRXCT960090 of the European Union, and by an Acción Integrada Hispano-Portuguesa. One of use (S.D.R.) thanks Borut Bajc for discussions and correspondence.

Appendix A

We will give here the explicit expressions for the various amplitudes referred to in the text. For A_{SM}, A_h and A_k we have [15]

$$A_{\mathrm{SM}} = A_W + A_F, \tag{A.1}$$

where

$$A_W = 4\cos\theta_W \left[(3 - \tan\theta_W^2)\, J_1(M_Z, M_H, M_W) + \left(-5 + \tan_W^2\theta_W - \frac{1}{2}\frac{M_H^2}{M_W^2}(1 - \tan\theta_W^2) \right) J_2(M_Z, M_H, M_W) \right], \tag{A.2}$$

$$A_F = \sum_f \frac{4g_V^f Q_f}{\cos\theta_W}\left[-J_1(M_Z, M_H, M_f) + 4J_2(M_Z, M_H, M_f)\right]. \tag{A.3}$$

In the previous equations we have introduced the functions J_1 and J_2 defined by

$$\begin{aligned} J_1(M_Z, M_H, M_W) &= -M_W^2 C_0(M_Z^2, 0, M_H^2, M_W^2, M_W^2, M_W^2), \\ J_2(M_Z, M_H, M_W) &= \frac{1}{2}\frac{M_W^2}{M_Z^2 - M_H^2}\left[1 + 2M_W^2 C_0(M_Z^2, 0, M_H^2, M_W^2, M_W^2, M_W^2)\right. \\ &\quad \left. + \frac{M_Z^2}{M_Z^2 - M_H^2}\left(B_0(M_Z^2, M_W^2, M_W^2) - B_0(M_H^2, M_W^2, M_W^2)\right)\right], \end{aligned} \tag{A.4}$$

where B_0 and C_0 are the Passarino–Veltman functions [16].

The amplitudes A_h and A_k are given by

$$\begin{aligned} A_h &= \frac{4\sin^2\theta_W}{\cos\theta_W}\left(\frac{\lambda_4 v^2 P_{i1} + \lambda_8 wv P_{i2}}{M_{h^\pm}^2}\right) J_2(M_Z, M_H, M_{h^\pm}), \\ A_k &= \frac{16\sin^2\theta_W}{\cos\theta_W}\left(\frac{\lambda_5 v^2 P_{i1} + \lambda_9 wv\ P_{i2}}{M_{k^{\pm\pm}}^2}\right) J_2(M_Z, M_H, M_{k^{\pm\pm}}). \end{aligned} \tag{A.5}$$

The amplitudes $\hat{A}_\phi$, $\hat{A}_h$ and $\hat{A}_k$ coming from the second set of diagrams with quartic vertices are

$$\begin{aligned} \hat{A}_\phi &= -4\cos\theta_W(1 - \tan^2\theta_W)\frac{1}{M_W}\frac{\lambda_7}{g} J_2(M_Z, M_{JJ}, M_W), \\ \hat{A}_h &= \frac{4\sin^2\theta_W}{\cos\theta_W}\frac{v\lambda_8}{M_{h^\pm}^2} J_2(M_Z, M_{JJ}, M_{h^\pm}), \\ \hat{A}_k &= \frac{16\sin^2\theta_W}{\cos\theta_W}\frac{v\,\lambda_9}{M_{k^{\pm\pm}}^2} J_2(M_Z, M_{JJ}, M_{k^{\pm\pm}}), \end{aligned} \tag{A.6}$$

where $M_{JJ}^2 = Q^2 = (q_2 + q_3)^2 = M_Z(M_Z - 2E_\gamma)$.

References

[1] For a review see, e.g. J.W.F. Valle, Prog. Part. Nucl. Phys. 26 (1991) 91, and references therein.

[2] A. Zee, Phys. Lett. B 93 (1980) 389; Phys. Lett. B 161 (1985) 141;
A.Yu. Smirnov and Zhi-jian Tao, Nucl. Phys. B 426 (1994) 415;
A.Yu. Smirnov and M. Tanimoto, hep-ph/9604370.

[3] K.S. Babu, Phys. Lett. B 203 (1988) 132.

[4] For a recent theoretical summary see talks by A.Yu. Smirnov at Neutrino 96, Helsinki, June 1996 and by J.W.F. Valle, at TAUP95, Nucl. Phys. B (Proc. Suppl.) 48 (1996) 137.

[5] For recent experimental discussions see talks by T. Kirsten, V. Gavrin, K. Lande and Y. Suzuki at Neutrino 96, Helsinki, June 1996.

[6] For a recent review see J.W.F. Valle, *in* Physics Beyond the Standard Model, AIP Conference Proceedings 359, p. 42, ed. J.C. D'Olivo, A. Fernandez and M.A. Perez, hep-ph/9603307; see also Nucl. Phys. B (Proc. Suppl.) 31 (1993) 221.

[7] J.T. Peltoniemi and J.W.F. Valle, Phys. Lett. B 304 (1993) 147.
[8] A. Joshipura and J.W.F. Valle, Nucl. Phys. B 397 (1993) 105.
[9] A. Lopez-Fernandez, J. Romão, F. de Campos and J.W.F. Valle, Phys. Lett. B 312 (1993) 240;
B. Brahmachari, A. Joshipura, S. Rindani, D.P. Roy and K. Sridhar, Phys. Rev. D 48 (1993) 4224;
A.S. Joshipura and S.D. Rindani, Phys. Rev. Lett. 69 (1992) 3269;
F. de Campos et al., proceedings of Moriond94, Electroweak Interactions and Unified Theories, Electroweak: 81-86 (QCD161:R4:1994:V.1) [hep-ph/9405382];
F. de Campos et al., Phys. Lett. B 336 (1994) 446.
[10] R. Akers et al. (OPAL collaboration), Z. Phys. C 64 (1994) 1.
[11] M. Mikheyev and A.Yu. Smirnov, Sov. J. Nucl. Phys. 42 (1986) 913;
L. Wolfenstein, Phys. Rev. D 17 (1978) 2369; D 20 (1979) 2634.
[12] Y. Chikashige, R. Mohapatra and R. Peccei, Phys. Rev. Lett. 45 (1980) 1926.
[13] J. Romão, J. Rosiek and J.W.F. Valle, Phys. Lett. B351 (1995) 497.
[14] F. de Campos, O.J.P. Eboli, J. Rosiek and J.W.F. Valle, Phys. Rev. D 55 (1997) 1316 [hep-ph/9601269].
[15] A. Barroso, J. Pulido and J.C. Romão, Nucl. Phys. B 267 (1986) 509.
[16] G. 't Hooft and M. Veltman, Nucl. Phys. B 153 (1979) 365;
G. Passarino and M. Veltman, Nucl. Phys. B 160 (1979) 151;
A. Axelrod, Nucl. Phys. B 209 (1982) 349.